energies

MDPI

Article

Master–Slave Based Hierarchical Control for a Small Power DC-Distributed Microgrid System with a Storage Device

Seung-Woon Lee and Bo-Hyung Cho *

Department of Electrical Engineering, Seoul National University 301-617, DaeHak-dong, GwanAk-gu, Seoul 151-742, Korea; dispell@snu.ac.kr

* Correspondence: bhcho@snu.ac.kr; Tel.: +82-2-880-1785

Academic Editor: Josep M. Guerrero

Received: 2 September 2016; Accepted: 25 October 2016; Published: 27 October 2016

Abstract: In this paper, we analyze one of the main drawbacks of droop control-based DC microgrid systems, and propose a novel control method to overcome this problem. Typically, DC microgrid systems use droop control techniques to enable communication independency and expandability. However, as these advantages are based on bus quality and regulation abandonment, droop-based schemes have limitations in terms of high bus impedance and bus regulation. This paper proposes a novel master–slave based hierarchical control technique for a DC distribution system, in which a DC bus signaling method is used to overcome the communication dependency and the expandability limitations of conventional master–slave control methods. The concept and design considerations of the proposed control method are presented, and a 1 kW simulation under a Powersim (PSIM) environment and hardware prototype—built to verify the system—is described.

Keywords: master–slave control with battery; DC microgrid with ESS; bus quality; communication-less master–slave

1. Introduction

Technological development and environmental protection concerns have led to the introduction of distributed energy resources (DERs)—such as gas- and wind-turbines and photovoltaic (PV) energy source—into microgrids [1–5]. Furthermore, the growth of PV into the most popular renewable energy source, as a result of its installation convenience, has helped to further the concept of the DC distribution system [6–10]. Not only do such systems bring the advantages of PV-to-DC grid energy conversion efficiency, but they also allow for the utilization of storage devices and digital loads [11]. For these reasons, DC microgrids have been studied under various application scenarios in an effort to find more efficient functionalities, structures, and control strategies.

As the technique for interfacing multiple energy sources at a DC distribution bus, the droop-based control method is widely used for energy management and bus voltage control [12–25]. Droop controls have many advantages, including communication independency and expandability, therefore, they can be widely used in microgrid environments requiring stable and reliable control. However, these benefits come at the cost of decreased bus quality owing to voltage regulation and transient response on the bus and, accordingly, incur high bus impedance [14–17,26]. These problems may result in difficulties of overall system optimization in terms of efficiency and stability.

Master–slave controls have many advantages in terms of bus quality and control, but face a critical drawback in terms of a communication link requirement. A conventional master–slave control depends on the power sharing and control ability of a communication link, and thus needs a high-speed communication link to a control system simultaneously [18,19]. Moreover, any communication delay or omission can reduce bus quality and system stability in general.

This paper proposes a novel master–slave control method that eliminates the need for a communication link. The proposed system utilizes the DC bus signaling (DBS) method [20] to replace additional communication, and controls the input power of device-stored energy instead of a load condition. A detailed concept, analysis, and design consideration are presented, and a 380 V, 1 kW simulation under a Powersim (PSIM) environment and hardware prototype were built to verify the suitability of the proposed system. This system is intended for use in DC home applications such as net zero energy houses [27,28] or nanogrid systems. Although the system has a small power capacity, it has the similar structure as a large-scale microgrid system, allowing for simplified system analysis and verification. As bus voltage regulation is more difficult with a single-phase power factor correction (PFC) circuit, thus such a circuit is used here to demonstrate the effectiveness of the proposed control method.

2. Structure and Operational Principles of the Proposed Master–Slave Method

Figure 1 shows the structure of the proposed DC distributed microgrid system. The DER consists of a PV panel, utility grid, battery, and load, and is connected to a DC bus using a renewable interface unit (RIU), grid interface unit (GIU), storage interface unit (SIU), and a load converter. Detailed parameters and system design are presented in Section 4.

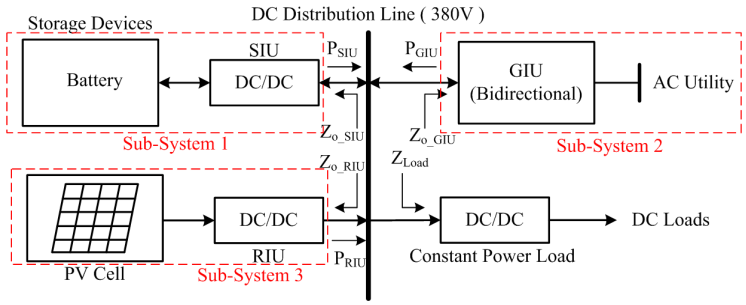

Figure 1. Block diagram of the proposed (DC) distributed microgrid system.

The primary purposes of a microgrid system are (1) to effectively operate and manage the DER, and (2) to maintain a stable bus voltage for supplying energy to the load. To satisfy these conditions, the master unit controls the bus voltage and slave units in order to supply power to the bus. Under a conventional control scheme, the slave units must be able to sense power-sharing information from the master unit or central controller. Using the DBS method, it is possible to eliminate the need for such communication links in the master–slave control; instead, the bus voltage is controlled using a predetermined DBS curve to change the power-sharing ratio of each interface unit. Thus, the master unit controls bus voltage using energy stored in a battery that is applied by the slave units using bus voltage information.

Figure 2 shows a control flow chart of the proposed system and key operation of the DBS-adapted communication-less master–slave control method. Figure 2a is a simplified control flow chart. The controllers are separated by a master unit and slave units, and the master unit controls bus voltage using the battery state-of-charge (*SoC*) level [22]. The slave units can be classified as controllable slave unit and uncontrollable slave unit. The renewable energy sources (e.g., PV panels) are used to control input voltage rather than bus voltage in order to generate maximum power, which eliminates arbitrary input power control. Thus, renewable energy sources requiring a maximum power point tracking (MPPT) algorithm are considered to be uncontrollable in this study. The slave units that can control generating power using the input or output inductor current are considered to be controllable slave units.

Figure 2b illustrates the operational principles of the proposed system. The master unit controls the bus voltage following Equation (1):

$$V_{Bus} = V_{Bus\_\text{default}} - K_m \times (SoC - SoC_{\text{nominal}}) \quad (1)$$

The bus voltage (V_{Bus}) changes linearly as the product of the battery *SoC* and the master coefficient K_m, which determines the correlation between the DC bus voltage and the battery *SoC*, and can be expressed as Equation (2):

$$K_m = \frac{V_{Bus.\max} - V_{Bus.\min}}{SoC_{\max} - SoC_{\min}} \quad (2)$$

The minimum and maximum range of the DC bus voltage and battery *SoC* level can be determined from the system design levels. Detailed parameters and a design guide are presented in Section 4.

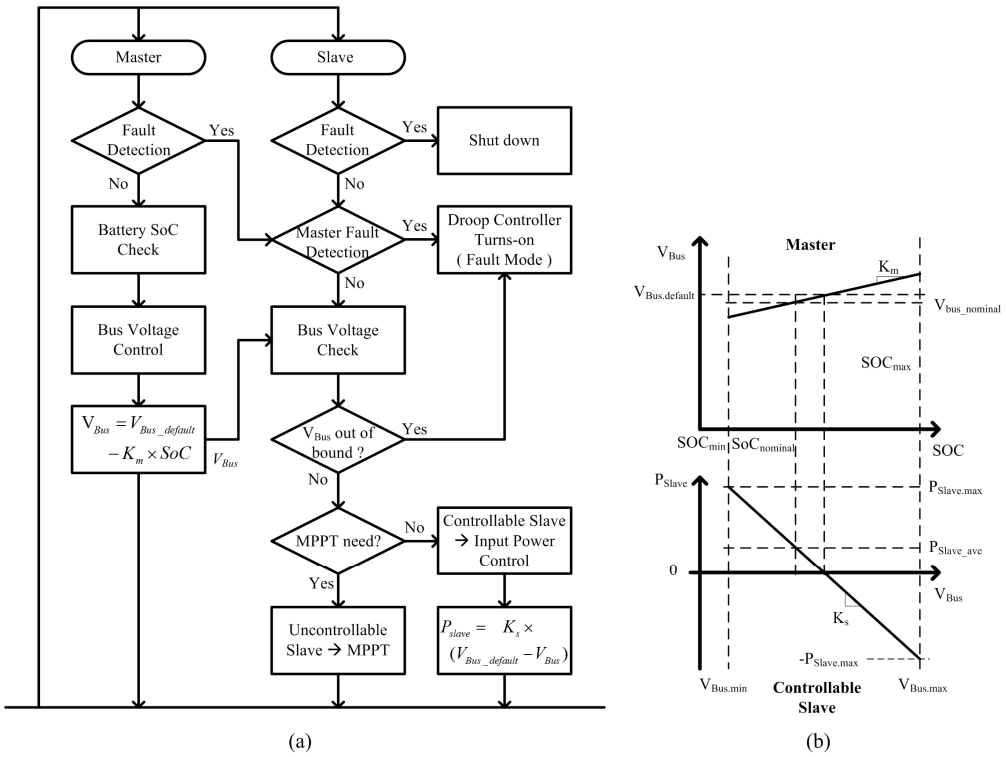

Figure 2. (**a**) Operational flow chart and (**b**) design principle of the proposed communication-less master–slave control method.

The slave coefficient K_s determines the power-sharing ratio of the system. Each slave unit senses bus voltage and controls its input power using its own predetermined K_s curve, which can be expressed as Equation (3):

$$K_s = -\frac{2P_{slave.\max}}{V_{Bus.\max} - V_{Bus.\min}} \quad (3)$$

The master and slave coefficients K_m and K_s can be designed as nonlinear functions. The voltage level signaling for the master unit and the power level signaling for a slave unit can take a nonlinear form that allows the DERs to be scheduled in various conditions. Figure 3 illustrates various K_m and K_s design cases for scheduling different power ratings of the master and slave units in a DC distributed microgrid system.

Using voltage level signaling, the DER energy scheduling can be designed to follow the battery *SoC* level. Similarly, the slave units can control their generating power based on the battery status. Figure 3 shows small and large K_s cases, respectively, for handling the battery depending on the *SoC*

range. In case (a), the battery is freely used over the 30%–70% *SoC* level, and the slave units charge and discharge the battery in states 1 and 3, respectively. In case (b), the slave units supply energy to the battery more sensitively, but the battery use range is more limited. Thus, a large K_s design can be adopted to maintain battery energy for standalone operation or islanding condition, while a small K_s design can be used for net zero energy building in order to decrease interference from the utility grid.

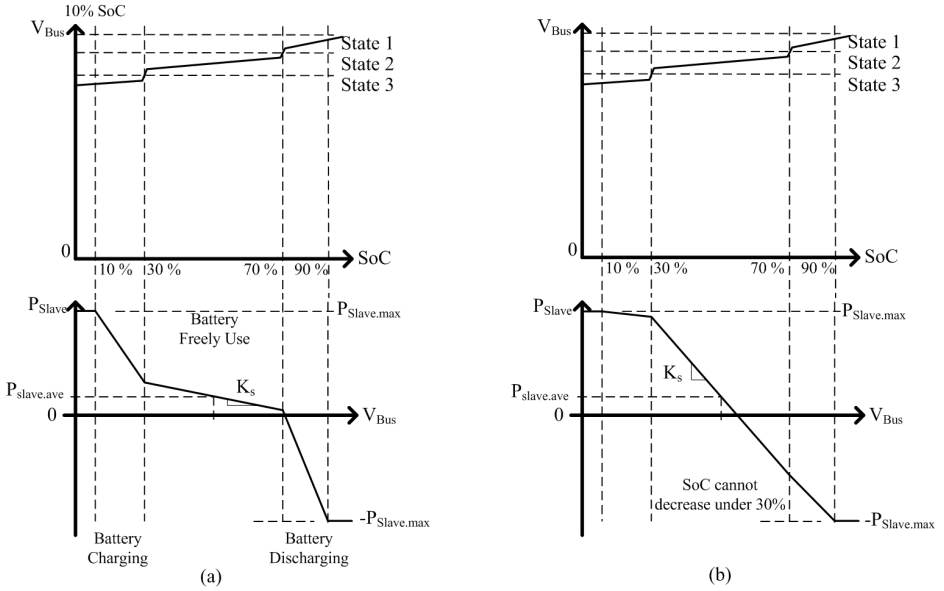

Figure 3. Nonlinear K_m and K_s curve designs of the proposed master–slave control method using (**a**) small K_s and (**b**) large K_s cases.

3. Master–Slave-Based Hierarchical Control Method

In a controlling DC distributed microgrid system, a hierarchical control structure is needed to satisfy ANSI/ISA-95. A detailed structure should be divided into more than three levels [13,21,23], but here, we will use two levels for simplicity (Figure 4). The controllers are separated into a local (low level) and central controller (high level), which are both connected with a low-speed communication link with the following functionalities:

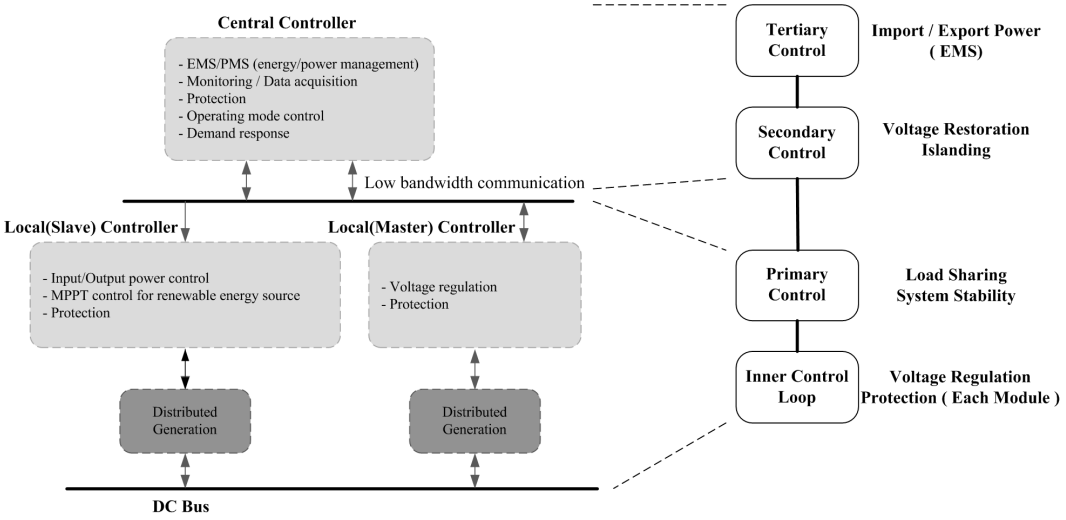

Figure 4. Control structure of the proposed method.

- Local Controller (inner control loop + primary control): bus voltage regulation, current and voltage control loop design, system stability issues, protection of each module, etc.
- Central Controller (secondary control + tertiary control): energy management of system, supply and demand prediction, bus quality control using bus voltage regulation, etc.

The local controller include all functions in each interface unit not involving communication, while the central controller manages additional algorithms for improving power quality and energy management using a communication link. Detailed designs of the local controller and central controller functions are presented as follows

3.1. Local Controller

As mentioned in Section 2, the local controller can be classified as a master, a controllable slave, or an uncontrollable slave unit. The design and function of an uncontrollable slave unit are identical to those of a conventional MPPT controller and, therefore, will be ignored in this paper.

Figure 5 shows a controller block diagram of the master and slave units. External signals v_{ref_ext} and i_{ref_ext} from the central controller direct voltage restoration and other functions. The master controller is similar to a conventional droop control, except that the droop gain is replaced with K_m based on the battery *SoC* level. The battery *SoC* level could be delivered from the central controller, but this would require additional communication by the master controller; hence, the SIU is preferred as a master unit. The SIU is directly connected to the battery, and therefore senses the battery output voltage in order to instantly calculate the battery *SoC* level [22]. Moreover, a DC–DC converter that compares with the GIU can be designed to have a faster voltage controller bandwidth than an AC–DC rectifier. The voltage loop bandwidth of a PFC circuit is often selected to be under 20 Hz in order to avoid 120 Hz distortion from the utility grid; as the performance of a master–slave system is determined by the controller bandwidth of the master unit, it is advantageous to select the SIU as a master in order to obtain higher DC bus quality.

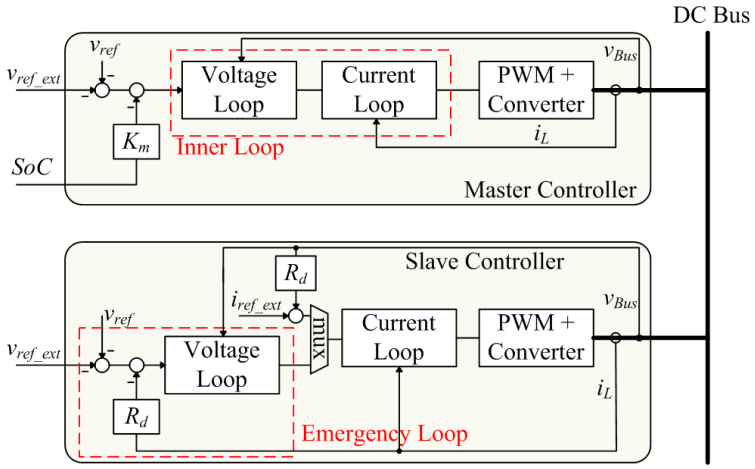

Figure 5. Local controller of the proposed method.

The slave controller in Figure 2 requires an emergency loop for fault operation; it operates only when the output voltage cannot be controlled by the master unit, and thus does not operate under the normal operating condition.

3.2. Central Controller

Nearly all functions of the central controller under the proposed method are similar to the functions of a conventional droop-based hierarchical controller [13]; they differ only in terms of the standard point compensation and modified bus voltage regulation functions.

Standard point compensation is needed to amend daily load and generation profile changing. In this method, the daily average power of the slave units affects the nominal bus voltage $V_{Bus\_nominal}$ (Figure 2b). Thus, nominal voltage restoration is required for the daily profile, which is changed by factors such as weather, temperature, and daylight condition, and the central controller must be able to monitor and make daily predictions in order to compensate for such changes. Voltage restoration is also required for bus regulation. Under the droop-based hierarchical control technique used by the proposed method, bus voltage is changed based on the battery *SoC* and, therefore, external compensation from a central controller is needed. Figure 6 shows the standard point and voltage restoration concept employed by the proposed system.

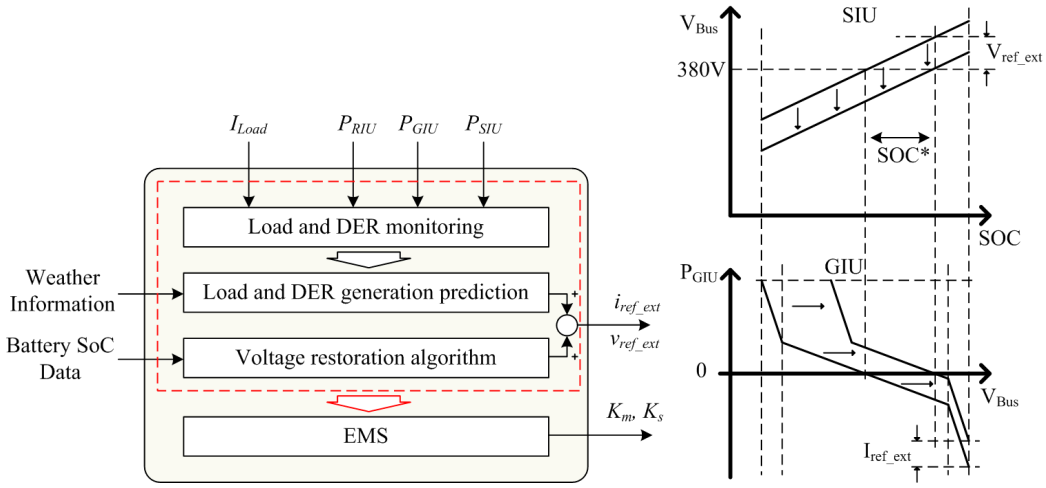

Figure 6. Central controller block diagram and DC bus voltage restoration concept of the proposed master–slave control method.

The master and slave DBS curve can be changed using V_{ref_ext} and I_{ref_ext} as shown in Figure 6. As the battery *SoC* is changed discontinuously, it can be easily compensated using Equations (4) and (5):

$$V_{ref\_ext} = K_m \times SoC^* \tag{4}$$

$$I_{ref\_ext} = \frac{K_s \times V_{ref\_ext}}{V_{Bus}} \tag{5}$$

Using the same reasoning, the standard point compensation can be added to extend Equation (5):

$$I_{ref\_ext}{}^* = \frac{K_s \times V_{ref\_ext}}{V_{Bus}} + \frac{P_{Slave\_ave}}{V_{Bus}} \tag{6}$$

Applying the values calculated in Equations (4) and (6) based on the external references in Figure 6, generating power control in the controllable slave units is possible without changing the DC bus voltage.

4. Simulation and Experimental Results

To investigate the effectiveness of the proposed method, a rated 380 V, 1 kW system was designed and implemented under both a simulation and a hardware environment. The system architecture is shown in Figure 7, and the hardware and controller parameters are specified in Table 1.

The GIU and SIU were designed together as a bidirectional circuit, with the SIU playing the master role. Output capacitors for each subsystem in Figure 1 were designed to have output voltage ripples of less than ±5 V. A detailed battery specification is provided in the Appendix of this paper.

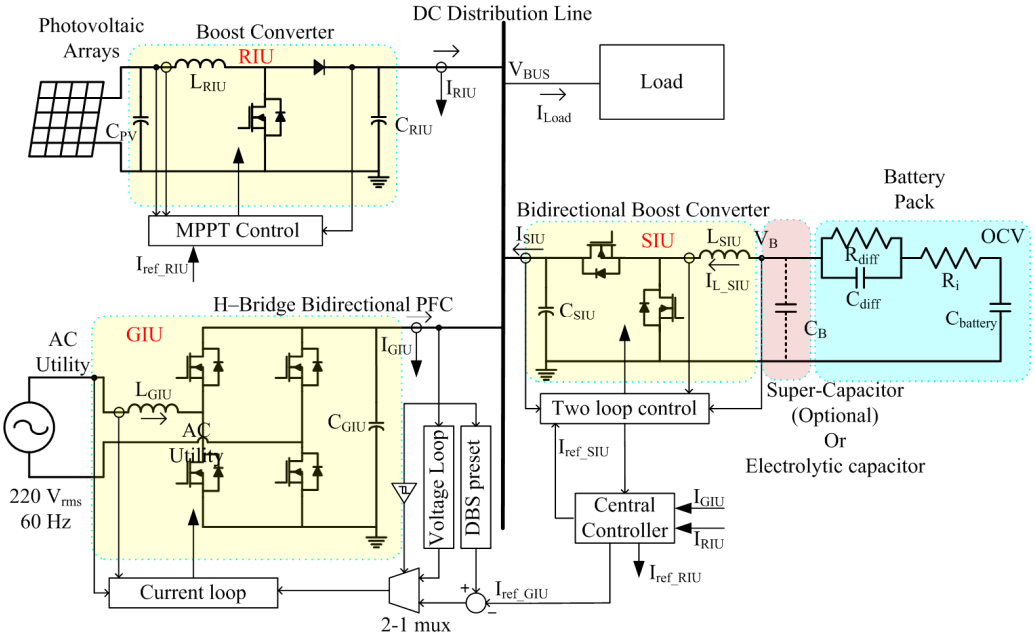

Figure 7. System architecture of the proposed DC distribution system.

Table 1. Hardware specification.

Unit Type	Symbol	Value	Note
GIU	f_{sw_GIU}	18 kHz	Switching frequency
	L_{GIU}	4 mH	-
	C_{GIU}	1 mF	-
	f_{BW_GIU}	1 kHz	Cut-off frequency of current controller
SIU	f_{sw_SIU}	50 kHz	Switching frequency
	L_{SIU}	740 µH	-
	C_{SIU}	47 µF	-
	C_B	100 µF	-
	f_{BW_SIU}	700 Hz	Cut-off frequency of voltage controller
Battery	OCV	150–240 V	Open circuit voltage range
	R_i	4.115 Ω	-
	R_{diff}	1.453 Ω	-
	C_{diff}	258.52 F	-
	$C_{battery}$	15,600 F	-
RIU	f_{sw_RIU}	50 kHz	Switching frequency
	C_{PV}	100 µF	-
	C_{RIU}	100 µF	-
	L_{RIU}	500 µH	-
	f_{BW_RIU}	450 Hz	Cut-off frequency of MPPT voltage controller
PV	V_{PV}	200 V	Open circuit voltage
		150 V	MPP voltage
	I_{PV}	8.4 A	Short circuit current
		7 A	MPP current

4.1. Simulation Results

The simulation was conducted to produce both short-term and long-term characteristics of the proposed control method. As short-term characteristics, the bus voltage ripple and transient response of the system was illustrated and compared with a conventional droop control system in order to verify the effectiveness of the proposed system in terms of bus regulation and dynamic properties.

As a long-term simulation, the power sharing of the master and slave units was demonstrated in order to verify the validity of the proposed communication-less master–slave control method.

Figure 8 shows steady-state comparisons between a conventional droop control method and the proposed master–slave control method. In both cases, the total load is 1 kW, and the GIU generates 90% power in order to identify maximum bus voltage ripple. At the same controller bandwidth and hardware design, the bus voltage ripple of the proposed method is approximately 4.7 V, while that of the droop control method is approximately 8.3 V.

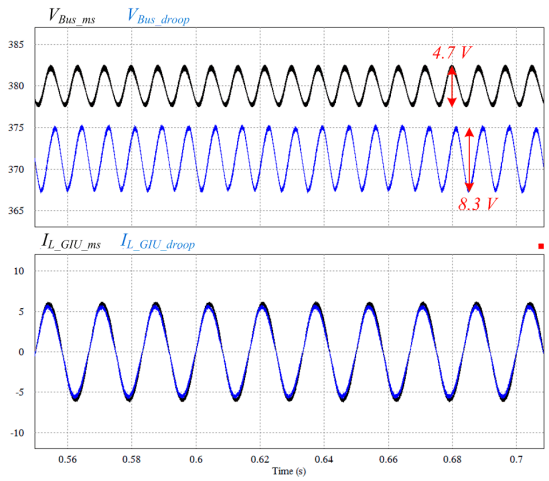

Figure 8. Steady-state simulation comparisons between a conventional droop control method and the proposed master–slave control method.

This difference arises from an impedance clamping problem in the droop control method. As shown in the small-signal block diagram in Figure 9a, droop gain is added in the control loop and clamps the low- and high-frequency output impedance of the converter, as shown in Figure 9b. The droop gain $\boldsymbol{R_d}$ clamps the bus impedance of the SIU, and interrupts its dynamic property in all regions.

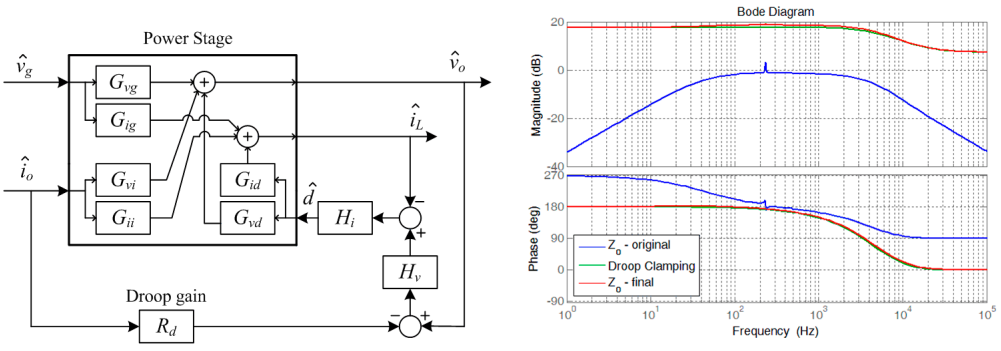

(a) (b)

Figure 9. (**a**) Small-signal block diagram of the storage interface unit (SIU) and (**b**) the output impedance bode diagram of the SIU in the droop control system.

Because the 120 Hz ripple from the utility side can be considered an external disturbance in the SIU side, this impedance clamping problem completely divides the regulation property of each unit. By contrast, the proposed method has no impedance clamping problem in any subsystem, and thus the equivalent bus impedance of the microgrid system can be compared as shown in Figure 10a. The calculated bus impedance of the proposed control method at 120 Hz is −2.7 dB, which means that

the bus voltage ripple of the DC microgrid system is compensated into 0.73 times the 120 Hz current disturbance, thereby satisfying the bus voltage ripple in Figure 9 of 4.7 V, with a 6.5 A peak current in the inductor current of the GIU.

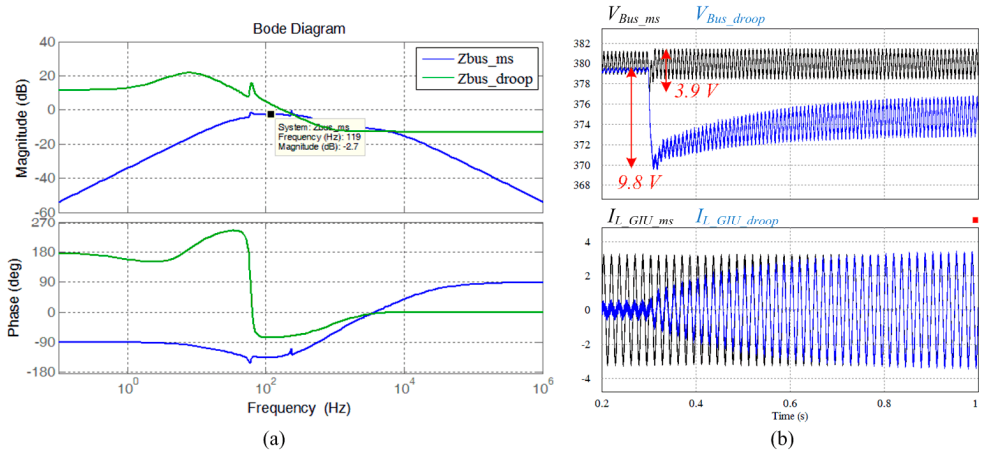

Figure 10. Comparisons between (**a**) equivalent bus impedance bode diagram and (**b**) simulation waveforms at step load changing condition.

Similarly, the simulation results of the step-load changing comparison shown in Figure 10b illustrate the advantages of the proposed control method. The figure shows a comparison of the transient characteristics of the bus voltage at load changes from 100 W to 1 kW at time 0.3 s. The transient response is much smaller and faster in the proposed method, as the master unit, the SIU, can be considered an additional shunt regulator [14].

The results of the long-term simulations are shown in Figure 11 as the bus voltage, battery *SoC*, and output current of the proposed method with a downscaled battery capacity (the battery *SoC* level changes too slowly with an original battery status to identify the characteristics of the proposed method).

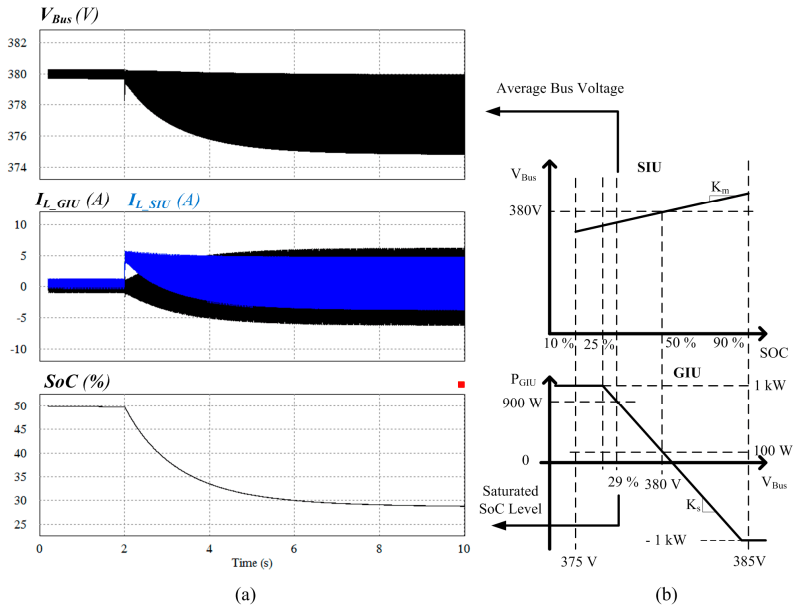

Figure 11. (**a**) Simulation waveforms at step-load changing condition with the battery state-of-charge (*SoC*) varying, and (**b**) master and slave curve design of the system.

Figure 11a shows the long-term simulation results with battery *SoC* variation. The battery capacity is changed at a 1/14,400 scale and the load changes from 100 W to 900 W at 2 s. The master and slave curve is designed as shown in Figure 11b and Table 2.

Table 2. Master and slave curve design values of the simulation.

Symbol	Value	Note
K_m	0.125	Master coefficient
K_s	−2	Slave coefficient
$V_{bus\_nominal}$	380 V	Nominal bus voltage
$P_{GIU.ave}$	100 W	Standard point value

In the simulation results, the GIU does not respond to the load changing and, therefore, the SIU immediately and solely covers the entire load. Thus, the battery *SoC* decreases through battery discharge and V_{Bus} changes following the master DBS curve design. In the same manner, the generation power of the GIU changes slowly and becomes saturated at a 29% *SoC* level. Saturating the battery *SoC* level takes approximately 8 s, as opposed to a calculated value of approximately 32 h at the original battery capacity.

4.2. Experimental Results

To verify the suitability of the proposed control method, short-term experimental hardware was built and tested. Because the battery capacity would otherwise overly prolong the experiment, the battery *SoC* level was changed artificially using an external signal.

Figure 12 shows the experimental waveforms of the step-load changing condition corresponding to those in Figure 10b. To check the bidirectional operation of the SIU, the load was changed from 1 kW to 0 W, and the GIU generated nearly 1 kW of power.

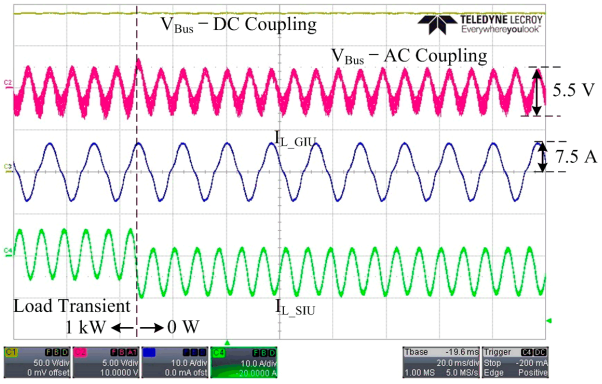

Figure 12. Experimental waveforms of the step-load changing condition.

As a result, an inductor current of the SIU changed to a negative value and charged the battery with 1 kW of instantaneous power. A measured bus voltage ripple of 5.5 V well-matched with the 7.5 A peak-to-peak inductor current of the GIU with a designed bus impedance of −2.7 dB.

Figure 13a shows the experimental waveforms of the proposed system when the battery *SoC* level is changed from 10% to 90% artificially. As shown by the red line, V_{Bus} changes from 375 V to 385 V as a result of the external battery *SoC* signal, and P_{GIU} changes from 1 kW to −1 kW, accordingly. The load condition does not change in this case, and I_{L_SIU} charges and discharges the battery according to I_{GIU} based on the dotted standard point. Figure 13b shows the same experimental result with DC voltage restoration; the bus voltage does not change, but I_{GIU} changes by the same amount as in Figure 13a.

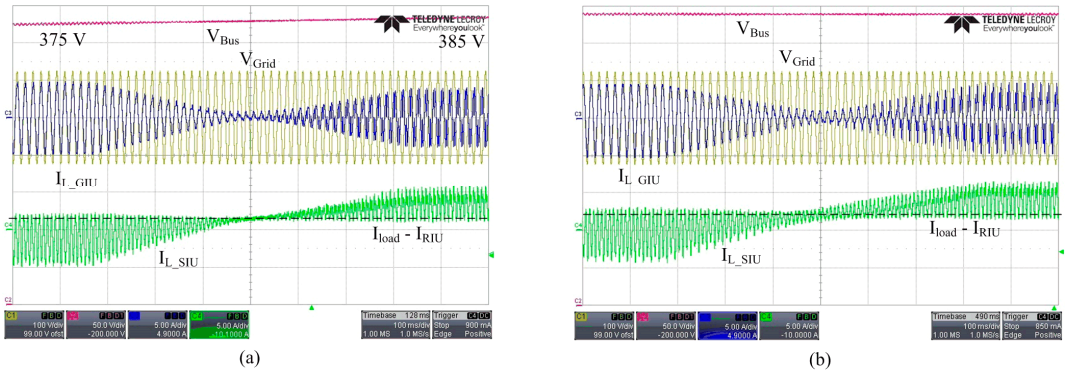

Figure 13. Experimental waveforms of the proposed system when the battery *SoC* level changes from 10% to 90% (**a**) without voltage restoration and (**b**) with voltage restoration.

5. Conclusions

A DC distribution system controlled by a communication-free master–slave-based hierarchical control method is presented in this paper. Although droop control has many drawbacks, including low frequency impedance clamping problems and a comparatively slow transient response, there has not been any previous widespread use of master–slave control in microgrid systems, owing to the communication dependency and low expandability of such systems. The proposed master–slave technique utilizes the DBS method to operate freely without communication in order to overcome these drawbacks. By replacing the droop control technique with the proposed master–slave technique, a DC distributed microgrid system can operate autonomously without distinction between grid connecting and islanding conditions. Moreover, the transient response of bus voltage is accelerated because of the presence of a high voltage bandwidth master unit. The concept and control strategies for the proposed control method were presented and analyzed in this paper, along with a voltage restoration method for more efficient and effective system design, and design considerations were discussed. The results obtained using 1 kW simulation and hardware modules operating from a 380 V DC bus demonstrate the feasibility of the proposed method.

Acknowledgments: This work was supported by the Korea Institute of Energy Technology Evaluation and Planning (KETEP) and the Ministry of Trade, Industry & Energy (MOTIE) of the Republic of Korea (No. 20151210200080).

Author Contributions: Seung-Woon Lee collected and analyzed the data and performed overall simulation and experiment. Bo-Hyung Cho contributed by overall technical suggestions. All the authors contributed to the writing of the final research paper.

Conflicts of Interest: The authors declare no conflict of interest.

Abbreviations

The following abbreviations are used in this manuscript:

GIU	Grid Interface Unit.
SIU	Storage Interface Unit.
RIU	Renewable Interface Unit.
P_{GIU}	Power transferred through GIU
P_{SIU}	Power transferred through SIU
P_{RIU}	Power transferred through RIU
P_{GIU_ave}	Daily average power transferred through GIU
V_{Bus}	DC bus voltage
$V_{Bus\_nominal}$	Daily nominal dc bus voltage
G_{vg}	Small signal transfer function of input voltage to output voltage
G_{ig}	Small signal transfer function of input voltage to inductor current

G_{vi}	Small signal transfer function of output current to output voltage
G_{vd}	Small signal transfer function of duty to output voltage
G_{id}	Small signal transfer function of duty to inductor current
G_{ii}	Small signal transfer function of output current to inductor current
H_i	Current loop controller function
H_v	Voltage loop controller function
R_d	Droop gain
G_{vi_closed}	G_{vi} when current and voltage loop are closed
R_{d_closed}	R_d when current and voltage loop are closed
T_i	Current loop gain
T_v	Voltage loop gain
Z_o	Output impedance
Z_{o_RIU}	Output impedance of the RIU
Z_{o_SIU}	Output impedance of the SIU
Z_{o_GIU}	Output impedance of the GIU
f_{sw}	Switching frequency of the converter
f_o	Frequency of utility grid
C_o	Output capacitor
I_{L_GIU}	Inductor current of GIU
I_{L_SIU}	Inductor current of SIU
I_{Load}	Total load current
I_{SIU}	Output current of SIU
I_{GIU}	Output current of GIU
I_{RIU}	Output current of RIU
f_{BW}	Closed loop controller bandwidth.

Appendix

Battery pack specification

1. Cell: ICR18650-26F, Samsung SDI

Typical voltage: 3.7 V
Maximum voltage: 4.45 V
Minimum voltage: 2.97 V
$C_{battery}$: 421,200 F
R_i: 0.1524 Ω
R_{diff}: 0.0538 Ω
C_{diff}: 6980 F
Capacity: 2.6 Ah-9.62 Wh

2. Pack: 54 Series-2 Parallel Stack

Typical voltage: 200 V
$C_{battery}$: 15,600 F
R_i: 4.1148 Ω
R_{diff}: 1.4526 Ω
C_{diff}: 258.5185 F
Capacity: 5.4 Ah-1 kWh

References

1. Bloemink, J.M.; Green, T.C. Benefits of Distribution-Level Power Electronics for Supporting Distributed Generation Growth. *IEEE Trans. Power Deliv.* **2013**, *28*, 911–919. [CrossRef]
2. Driesen, J.; Katiraei, F. Design for Distributed Energy Resources. *IEEE Power Energy Mag.* **2008**, *6*, 30–40.
3. Pepermans, G.; Driesen, J.; Haeseldonckx, R.; D'haeseleer, W. Distributed generation: Definition, Benefits and Issues. *Energy Policy* **2005**, *33*, 787–798. [CrossRef]

4. Hatziargyriou, N.; Asano, H.; Iravani, R.; Marnay, C. Microgrids. *IEEE Power Energy Mag.* **2007**, *5*, 78–94. [CrossRef]
5. Sechilariu, M.; Locment, F.; Wang, B. Photovoltaic Electricity for Sustainable Building Efficiency and Energy Cost Reduction for Isolated Microgrid. *Energies* **2015**, *8*, 7945–7967. [CrossRef]
6. Hammerstrom, D.J. AC versus DC Distribution Systems-Did We Get It Right? In Proceedings of the Power Engineering Society General Meeting, Tampa, FL, USA, 24–28 June 2007; pp. 1–5.
7. Huey, P.; Lo, E.; Pong, B. DC Electrical Distribution Systems in Buildings. In Proceedings of the International Conference on Power Electronics Systems and Applications, Hong Kong, China, 12–14 November 2006; pp. 115–119.
8. Karlsson, P. DC Distributed Power Systems: Analysis, Design and Control for a Renewable Energy Systems. Ph.D. Thesis, Department of Industrial Electrical Engineering and Automation, Lund University, Lund, Sweden, 2002.
9. Pratt, A.; Kumar, P.; Aldridge, T.V. Evaluation of 400 V DC Distribution in Telco and Data Centers to Improve Energy Efficienty. In Proceedings of the International Telecommunications Energy Conference, Rome, Italy, 30 September–4 October 2007; pp. 32–37.
10. Baran, M.E.; Mahajan, N.R. DC Distribution for Industrial Systems: Opportunities and Challenges. *IEEE Trans. Ind. Appl.* **2003**, *39*, 1596–1601. [CrossRef]
11. Seo, G.S.; Baek, J.B.; Choi, K.S.; Bae, H.; Cho, B. Modeling and Analysis of DC Distribution Systems. In Proceedings of the International Conference on Power Electronics and ECCE Asia, Jeju, Korea, 30 May–3 June 2011; pp. 223–227.
12. Johnson, B.K.; Lasseter, R.H.; Alvarado, F.L.; Adapa, R. Expandable multi-terminal DC Systems Based on Voltage Droop. *IEEE Trans. Power Deliv.* **1993**, *8*, 1926–1932. [CrossRef]
13. Guerrero, J.M.; Vasquez, J.C.; Matas, J.; de Vicuna, L.G.; Castilla, M. Hierarchical Control of Droop-Controlled AC and DC Microgrids—A General Approach toward Standardization. *IEEE Trans. Ind. Electron.* **2011**, *58*, 158–172. [CrossRef]
14. Cao, X.; Zhong, Q.C.; Ming, W.L. Ripple Eliminator to Smooth DC-Bus Voltage and Reduce the Total Capacitance Required. *IEEE Trans. Ind. Electron.* **2015**, *62*, 2224–2235. [CrossRef]
15. Dong, D. AC-DC Bus-interface Bi-directional Converters in Renewable Energy Systems. Ph.D. Thesis, Electrical Engineering, University of Virginia Polytechnic Institute and State University, Blacksburg, VA, USA, July 2012.
16. Magro, M.C.; Mariscotti, A.; Pinceti, P. Definition of Power Quality Indices for DC Low Voltage Distribution Networks. In Proceedings of the Instrumentation and Measurement Technology Conference, Sorrento, Italy, 24–27 April 2006; pp. 1885–1888.
17. Electric Power Research Institute (EPRI). *DPQ Executive Summary*; EPRI: Pal Alto, CA, USA, 2003.
18. Tsikalakis, A.G.; Hatziargyriou, N.D. Centralized Control for Optimizing Microgrids Operation. *IEEE Trans. Energy Convers.* **2008**, *23*, 241–248. [CrossRef]
19. Luo, S.G.; Ye, Z.G.; Lin, R.L.; Lee, F.C. A classification and evaluation of paralleling methods for power supply modules. In Proceedings of the Power Electronics Specialists Conference, Charleston, VA, USA, 1 July 1999; pp. 901–908.
20. Schonberger, J.K. Distributed Control of a Nanogrid Using DC Bus Signaling. Ph.D. Thesis, Electrical and Electronic Engineering, University of Canterbury, Chiristchurch, UK, May 2005.
21. Cvetkovic, I. Modeling, Analysis and Design of Renewable Energy Nanogrid Systems. Master's Thesis, Electrical Engineering, Virginia Polytechnic Institute and State University, Virginia, VA, USA, July 2010.
22. Chun, C.Y.; Baek, J.; Seo, G.S.; Cho, B.H.; Kim, J. Current Sensor-less State-of-charge Estimation Algorithm for Lithium-Ion Batteries Utilizing Filtered Terminal Voltage. *J. Power Sources* **2015**, *273*, 255–263. [CrossRef]
23. Baochao, W.; Sechilariu, M.; Locment, F. Intelligent DC Microgrid with Smart Grid Communications: Control Strategy Consideration and Design. *IEEE Trans. Smart Grid* **2012**, *3*, 2148–2156.
24. Anand, S.; Fernandes, B.G.; Guerrero, J. Distributed Control to Ensure Proportional Load Sharing and Improve Voltage Regulation in Low-Voltage DC Microgrids. *IEEE Trans. Power Electorn.* **2013**, *28*, 1900–1913. [CrossRef]
25. Gavriluta, C.; Candela, J.I.; Rocabert, J.; Luna, A.; Rodriguez, P. Adaptive Droop for Control of Multiterminal DC Bus Integrating Energy Storage. *IEEE Trans. Power Deliv.* **2015**, *30*, 16–24. [CrossRef]

26. Whaite, S.; Grainger, B.; Kwasinsky, A. Power Quality in DC Power Distribution Systems and Microgrids. *Energies* **2015**, *8*, 4378–4399. [CrossRef]
27. Saberbari, E.; Saboori, H. Net-Zero Energy Building Implementation through a Grid-Connected Home Energy Management System. In Proceedings of the 19th Electrical Power Distribution Conference (EPDC2014), Tehran, Iran, 6–7 May 2014.
28. Aste, N.; Adhikari, R.S.; Del Pero, C. Photovoltaic Technology for Renewable Electricity Production: Towards Net Zero Energy Buildings. In Proceedings of the International Conference on Clean Electrical Power (ICCEP), Ischia, Italy, 14–16 June 2011.